Article

Research on Intelligent Design and Visualization of Gas Extraction Drilling Based on PSO–LSTM

Yongming Yin [1,2], Dacang Wang [2,*], Quanjie Zhu [3], Guangyu Yang [4,5], Xuexi Chen [6], Xiaohui Liu [6] and Yongfeng Liu [7]

1. China Academy of Safety Science and Technology, Beijing 100012, China
2. Cathay Safety Technology Co., Ltd., Beijing 100012, China
3. School of Emergency Technology and Management, North China Institute of Science and Technology, Sanhe 065201, China
4. Coal Mining Research Institute Co., Ltd. of CCTEG, Beijing 100013, China
5. State Key Laboratory of Coal Ming and Clean Utilization, Beijing 100013, China
6. School of Safety Engineering, North China Institute of Science and Technology, Sanhe 065201, China
7. School of Resources and Safety Engineering, Chongqing University, Chongqing 400044, China
* Correspondence: wdc15102587295@163.com

Abstract: Under the background of intelligent construction of coal mines, gas extraction design is still based on manual design, which is complex, time–consuming, and error–prone, and its automation degree needs to be improved. In order to solve this problem, taking the 1302 working face of a mine in Shanxi Province as the research object, this paper carried out relevant research. Firstly, the influencing factors of gas extraction were determined, and the influence rules of different parameters on the extraction effect were studied by numerical simulation. Secondly, an intelligent optimization method of gas extraction drilling parameters based on deep mining called the PSO–LSTM model, is proposed. This model uses the PSO algorithm to optimize the parameters of the LSTM model, so as to improve the accuracy of the LSTM model results. Finally, a quantitative expression algorithm of 3D spatial information of gas extraction drilling holes based on Python is proposed, which can automatically generate 3D spatial models of bedding or through gas extraction drilling holes using optimized drilling parameters and known 3D information of coal seams. This study shows that the results obtained using the PSO–LSTM model are the same as the drilling parameters obtained using numerical simulation, which verifies the accuracy of the PSO–LSTM model. According to the optimized drilling parameters, a 3D model of gas extraction drilling is quickly generated, which greatly reduces the tedious work of drawing construction drawings for coal mine enterprises and improves the intelligence level of coal gas extraction drilling.

Keywords: gas extraction; drilling parameter optimization; PSO–LSTM; 3D model; Python

1. Introduction

Coal mine gas extraction is a systematic engineering process that includes the design and construction of extraction drilling holes, coal seam anti–reflection, monitoring and testing, standard evaluation, and other links. The design of the drilling hole is the main basis of drilling construction. The scientific and rational design of the drilling holes directly affects the difficulty of drilling construction and the amount of engineering, as well as the later extraction efficiency. The design of extraction drilling must be considered from various factors. It is a complex decision–making process that is limited by various factors such as coal seam gas geological conditions, drilling construction environment, drilling machine drilling tool performance, and so on. It is necessary to balance various needs, such as gas extraction standards, drilling construction difficulty, and drilling amount, so that the drilling layout scheme can achieve the overall optimization state. At present, the design of coal mine gas extraction drilling is mainly based on manual work. In addition to the large

workload, which is time–consuming and laborious, there are also the following problems. First, the design basis of the drilling hole is unreasonable. In addition to the inaccurate knowledge of gas geological conditions, key parameters, such as the effective extraction radius of the drilling hole, are mainly obtained through experimental measurement or experience, which are static and inaccurate. When the extraction location is transferred, and the coal seam gas geological conditions change significantly, the drilling hole design cannot be effectively supported. Secondly, the borehole design is not fine enough, and the whole extraction area is designed according to the same conditions without fully considering the differences in coal seam gas geological conditions and the length of gas pre–extraction time at different locations in the region. This can easily cause the borehole arrangement to be too thin or too dense, resulting in poor extraction effect, substandard extraction, increased drilling projects, and shortage of mining replacement. Therefore, the development trend of gas extraction drilling intelligent design is to carry out research on gas extraction drilling intelligent design technology, realize the fine automatic design of drilling parameters, and make the drilling layout reasonably match the extraction conditions and demand.

In recent years, with people's attention to gas extraction, research in the field of gas extraction is also carried out continuously. The optimization design of gas extraction parameters includes a variety of methods. One is a field test and data analysis. Gas extraction tests with different technological parameters are carried out at the coal mine site [1–6]. The field test can directly reflect the gas extraction effect under actual production conditions and provide real and reliable data for the optimization of process parameters. The second is numerical simulation and simulation analysis. Numerical simulation software is used to simulate and analyze the gas extraction process, and its influence on the extraction effect is observed by changing different technological parameters (such as drilling hole layout, drilling spacing, drilling diameter, etc.) so as to determine the optimal parameter combination [7–12]. This method can intuitively show the gas flow law, provide a scientific basis for parameter optimization, and reduce the blindness and cost of the field test. The third is intelligent control to optimize technology, the application of sensors, data acquisition technology, cloud computing, and other advanced technologies, and the establishment of intelligent gas monitoring and control systems. Through real–time monitoring of the gas concentration and operation parameters of the extraction equipment, the extraction process parameters can be automatically adjusted to realize intelligent control [13–18]. Intelligent control can significantly improve the response speed and accuracy of gas extraction systems, reduce the risk of human error, and improve the safety and stability of the system. Later, different scholars carried out research on gas extraction from the aspects of pressure relief [19–21], blasting [22], hole sealing [23], etc., so as to optimize the drilling horizon and improve the gas extraction efficiency.

In addition, other predecessors have also made visual presentations on gas extraction research. Xu Xuezhan et al. [24] used 3D modeling software and numerical simulation software to simulate the high–efficiency gas extraction range and used 3D modeling software and numerical simulation software to carry out a three–dimensional visual simulation of the through–layer gas extraction process. In terms of 3D visualization, Zhang Jilin et al. [25] developed a 3D visualization analysis software system for coal mine drilling holes, which realized intelligent design, automatic mapping of gas extraction drilling holes, and display of drilling shapes in a 3D environment. However, this type of software does not have the ability to identify the hidden dangers of hole arrangement. Therefore, Fan Kai [26] established a three–dimensional effect display and analysis platform for gas extraction drilling holes and applied the system to Sihe Coal Mine, realizing the timely discovery and complete elimination of hidden dangers of hole arrangement. However, the above gas extraction visualization system is difficult to develop for low–level personnel and difficult to popularize. Based on this, Zhu Quanjie et al. [27] used Blender, Python, and other open–source programs to build a rapid generation platform for 3D mine models based on parametric modeling ideas. Easy to grassroots development again: Users only need to input key data information to realize the rapid generation of a tunnel 3D model.

In the context of smart coal mine construction, gas drainage, as a fundamental solution to coal mine gas disasters, will emerge as a pivotal technology for addressing the challenges of gas disaster prevention and control in deep mining, thereby enhancing safety standards for coal mine operations. It constitutes a vital component of smart coal mine development. At present, the intelligence level of coal gas drainage technology and equipment in China is still very low. Overall, it is in the initial stage, and there is an urgent need to integrate modern information technology into the field of coal gas drainage and gradually realize the information, automation, and intelligence of gas drainage. For the application scenarios of coal mine gas extraction borehole design, drainage system regulation and maintenance, and drainage standard evaluation, the technologies of mine big data, coal mine 5G, and artificial intelligence are fully adopted to break through the key technologies of dynamic transparent gas geology, drilling intelligent design, drainage pipe network autonomous regulation and fault diagnosis, and drainage standard intelligent evaluation. The development direction of intelligent gas extraction is to form intelligent equipment and systems with the ability of accurate perception, autonomous decision–making, and automatic adaptation, and realize less or even no human operation in the whole process of gas extraction. Because the design and layout of a gas extraction drilling field are affected by coal seam occurrence, geological anomalies (such as faults), gas content, engineering layout, and other factors, the design of a reasonable and effective gas extraction drilling hole directly affects the gas extraction effect. Conventionally, technicians design drilling parameters and carry out construction according to the requirements of the "Rules for the Prevention and Control of Coal and Gas Outburst" (2019 edition) and other requirements, combined with the actual situation of the mine. This process runs throughout the gas coal seam mining process; the workload is large, complex, and time–consuming. With the gradual advancement of intelligent construction in coal mines, automation and intelligent construction of gas extraction work are on the agenda, and the automatic design and three–dimensional display of gas extraction drilling will become an important research topic in this field.

Based on the development trend of gas extraction toward precision, efficiency, and intelligence, the key technologies of intelligent design and visual display of gas extraction drilling holes are proposed. The research contents include influencing factors of gas extraction, the intelligent calculation method of key parameters, visualization of optimized drilling parameters, etc. This research not only provides a new method for the intelligent design of gas extraction drilling and intelligent generation of construction three–dimensional drawings but also has a positive guiding role for parameter design and on–site construction in this field.

2. Analysis of Factors Affecting Gas Extraction

2.1. Analysis of Influencing Factors

The effective drainage radius is the key index for evaluating the gas drainage effect, which directly reflects the effective range of the gas drainage drilling hole. Clarifying the factors influencing the effective extraction radius is of great significance for optimizing the gas extraction process and improving the extraction efficiency, and can also provide a clear direction for numerical simulation research on gas extraction.

According to the radial flow field law of gas migration, the initial intensity expression of gas emission from the drilling hole is as follows [28]:

$$q_o = 2\pi m\lambda \frac{p_o^2 - p_l^2}{\ln \frac{R}{r_o}} \tag{1}$$

The borehole gas emission intensity at time *t* is expressed as follows [28]:.

$$q = q_0 e^{-\alpha t} \tag{2}$$

At time *t*, the total amount of gas extracted from the borehole is as follows [28]:

$$Q = \int_0^t q \, dt = \int_0^t q_0 e^{-\alpha t} dt = \frac{2\pi m \lambda (p_0^2 - p_l^2)(l - e^{-\alpha t})}{\alpha ln \dfrac{R}{r_o}} \qquad (3)$$

For the range where the length and width of the extraction area are *a* and *b* respectively, the gas extraction amount is [28]

$$Q_{Extraction} = \eta Q_{All} = \eta abm\gamma W \qquad (4)$$

The number of boreholes required to have an effective extraction radius *R* is [28]

$$N = \frac{a}{2R} \cdot \frac{b}{2R} = \frac{ab}{4R^2} \qquad (5)$$

From $Q_{Extraction} = NQ_{All}$, we can obtain [28]

$$R^2 = \frac{\pi \lambda (p_0^2 - p_1^2)(1 - e^{-\alpha t})}{2\alpha\eta\gamma W \ln \dfrac{R}{r_o}} \qquad (6)$$

where: η represents extraction efficiency, %; q_0 is the initial intensity of gas emission from the borehole, m³/(min·hm); α represents the attenuation coefficient of borehole gas flow, d^{-1}; *R* represents the effective influence radius of gas extraction, *m*; λ represents the permeability coefficient of coal seam, m²/(MPa²·d); p_0 is the initial pressure of coal seam gas, MPa; p_1 represents the gas pressure in the borehole, MPa; r_0 represents the borehole diameter, *m*; γ is the bulk density of coal, t/m³; *W* is the original gas content of coal seam, m³/t; *m* is the borehole length, m; P_{std} is standard atmosphere, MPa.

Through the analysis of Formula (6), we can gain insight into several core elements that affect the effective radius of extraction. Among them, the most important factors are the diameter of the drilling hole, the permeability of the coal seam, the initial gas pressure, the negative pressure of extraction, and the duration of extraction, which show a significant positive correlation with the effective extraction radius, which reveals a close relationship between them.

In the stage of coal seam gas pre–extraction, the three variables of drilling diameter, extraction negative pressure, and extraction time can be effectively regulated in the industrial production process. Therefore, with the help of advanced numerical simulation software, we can simulate how these controllable factors affect the effective extraction radius, which provides us with a deeper understanding of the extraction process and supports the optimization of the process.

2.2. Mesh Model and Coal Seam Parameters

In the 1302 working face of a mine in Shanxi Province, 94 mm drilling holes are used for gas extraction, the spacing of drilling holes is 5 m, the single arrangement of holes, and the extraction time is 120 days. A two–dimensional model with a length of 50 m and width of 5 m (as shown in Figure 1) was constructed using numerical simulation software to observe the effects of different parameters on the effective extraction radius. The parameters of the coal seam are shown in Table 1.
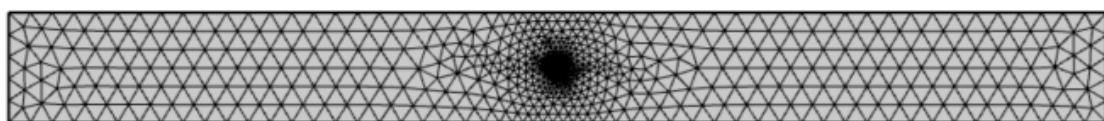

Figure 1. Single–hole extraction model grid.

Table 1. Parameter of coal seam.

Parameter	Parameter Value	Parameter	Parameter Value
Elastic modulus of coal	2.415×10^9 Pa	Density of gas	0.716 kg/m^3
Apparent density of coal	1380 kg/m^3	Initial gas pressure	1.53 MPa
Moisture content	1.53%	Limit adsorption gas capacity	15.53 m^3/t
Ash content	14.72%	Gas adsorption constant	1.32 MPa^{-1}
Initial porosity	5.45%	Gas dynamic viscosity coefficient	1.06×10^{-5} Pa·s
Initial permeability	1.74×10^{-16} m^2	Poisson's ratio	0.3

2.3. Influence of Different Parameters on Gas Extraction

In order to study the influence of different parameters on gas extraction, the following four groups of simulations were carried out:

(1) In the actual gas extraction process, the gas extraction cycle is generally three to four months, so this paper takes 30 d, 60 d, 90 d, and 120 d as the extraction period to carry out numerical simulations to study the change in gas pressure.

(2) Boreholes with diameters of 75 mm, 94 mm, 133 mm, and 143 mm were used for numerical simulation, and the change in gas pressure was observed to study the relationship between borehole diameter and effective extraction radius.

(3) In order to study the relationship between the effective extraction radius and hole spacing, the gas pressure changes were simulated when the hole spacing was 2, 3, and 4 times the effective extraction radius.

(4) In order to explore the relationship between the negative drainage pressure and the effective drainage radius, the negative drainage pressures of 10 KPa, 20 KPa, 30 KPa, and 40 KPa were used for numerical simulation, and the gas pressure changes among them were observed.

The cloud diagram of the gas pressure variation under different parameters is shown in Figure 2, and the variation trend of the effective extraction radius under different parameters is shown in Figure 3. According to Figures 2 and 3, when other conditions remain unchanged, the effective extraction radius increases with the increase in extraction time, drilling diameter, and extraction negative pressure. In a certain range of content, the larger the drilling spacing, the larger the effective extraction range; however, beyond a certain range, the effective extraction range will not increase. According to the simulation results, the maximum drilling spacing is 6 m.
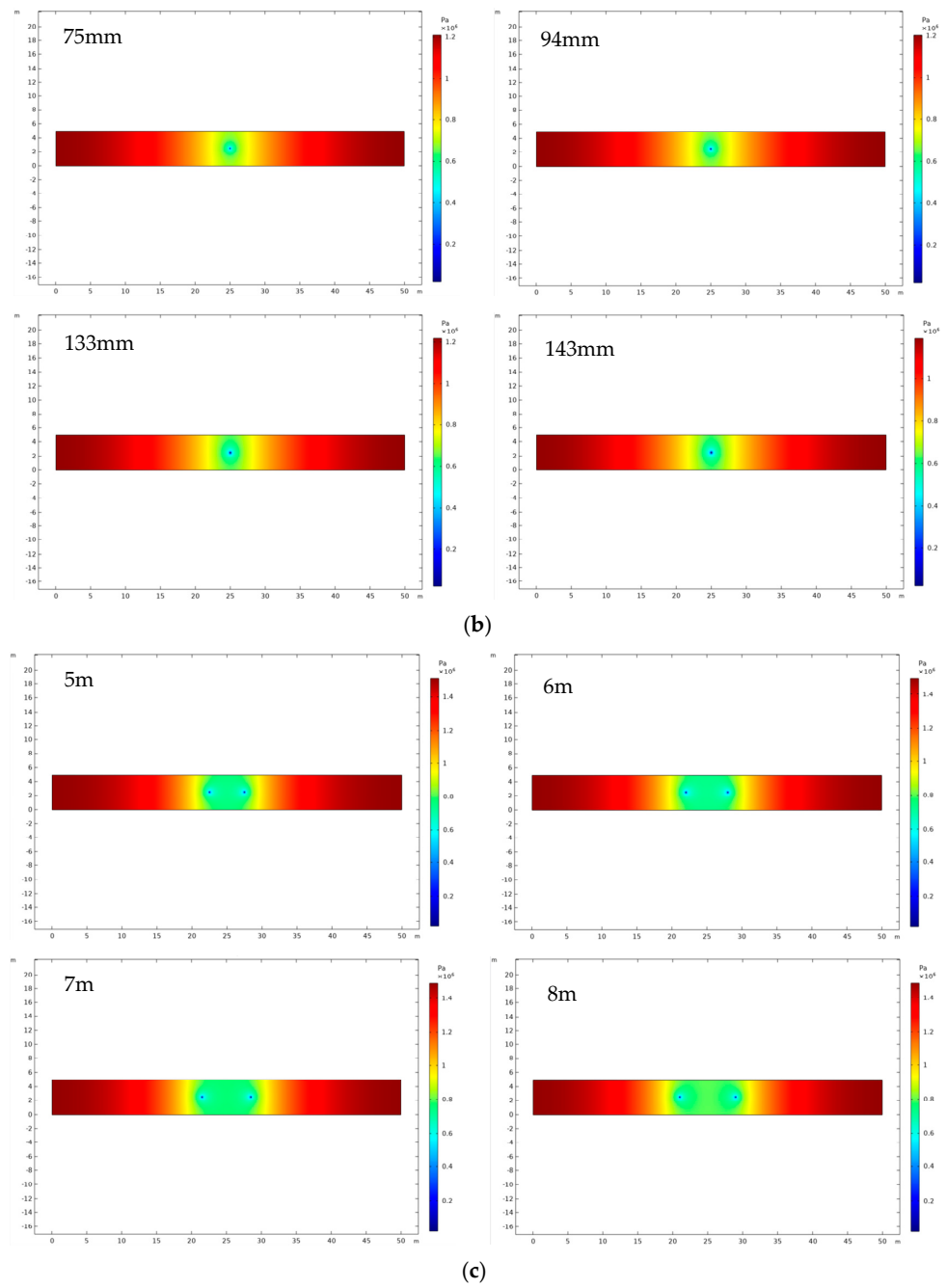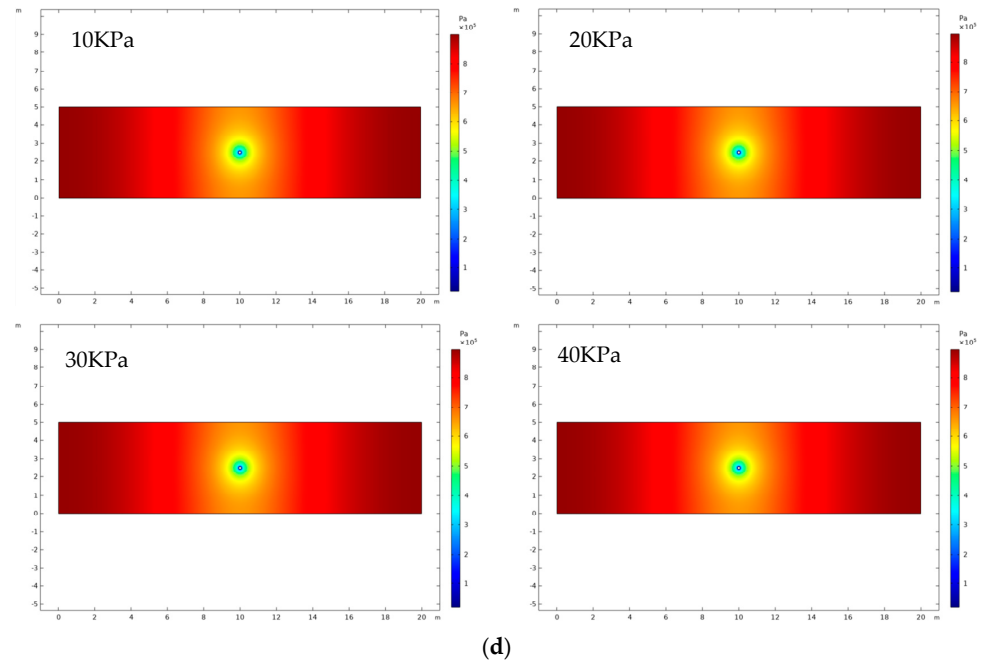

(a)

Figure 2. *Cont.*
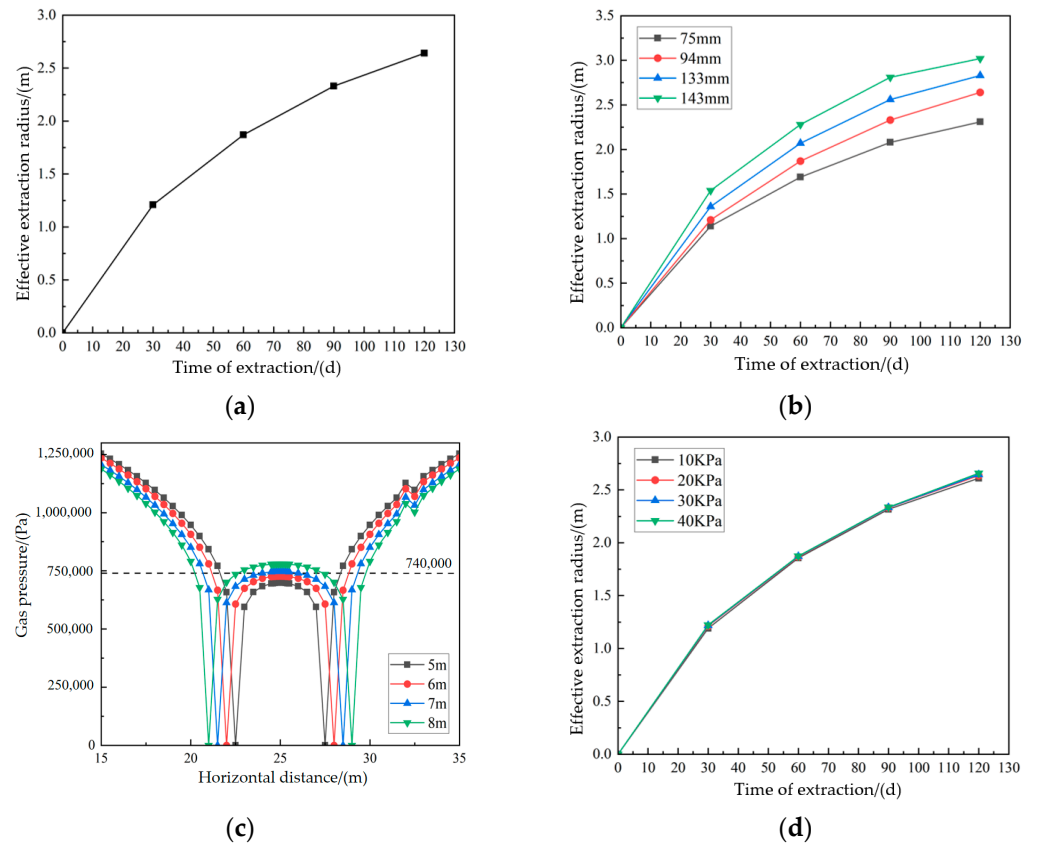
(**b**)

(**c**)

Figure 2. *Cont.*

(**d**)
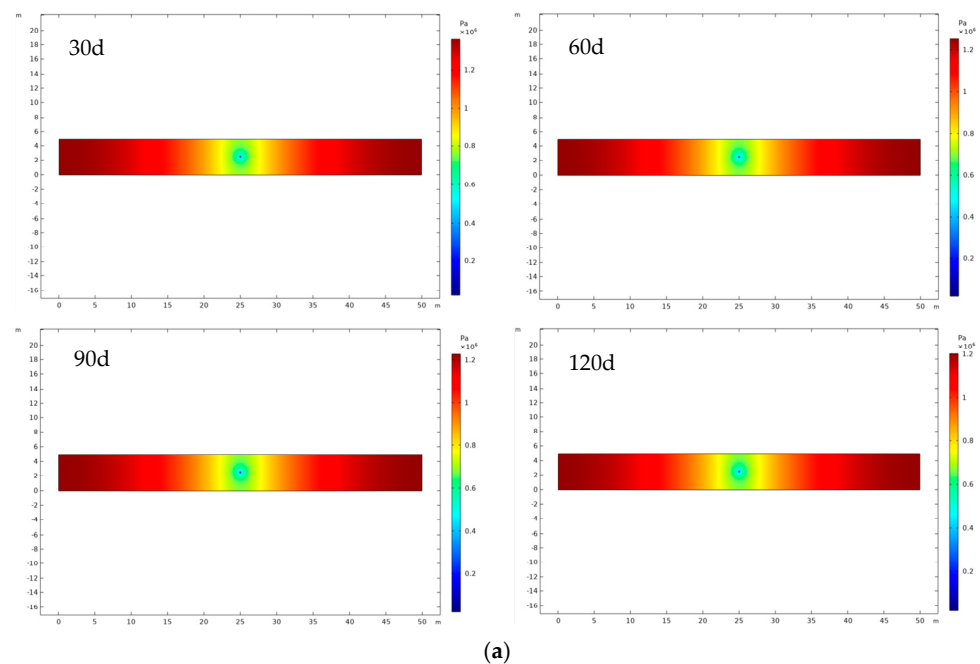
Figure 2. Cloud diagram of gas pressure variation under different parameters. (**a**) Different extraction time; (**b**) Different extraction diameters; (**c**) Different hole spacing; (**d**) Different suction negative pressure.

(**a**)

(**b**)

(**c**)

(**d**)

Figure 3. Variation trend of the effective extraction radius under different parameters. (**a**) Different extraction time; (**b**) Different extraction diameters; (**c**) Different hole spacing; (**d**) Different suction negative pressure.

3. Research Methods and Ideas of the Thesis

This paper first studies the influence of different drilling parameters on the effective extraction radius and then constructs a gas extraction parameter optimization model to predict drilling parameters. Finally, a 3D drilling model was constructed to realize the optimized 3D drilling visualization display. Specific implementation methods and ideas are as follows:

3.1. Parameter Optimization Algorithm (PSO–LSTM)

(1) PSO algorithm

The particle swarm optimization (PSO) algorithm is derived from research on bird predation behavior. The basic idea is to seek an optimal solution through mutual cooperation and information sharing among individuals within the group. In this algorithm, a massless particle is used to simulate an individual in a flock. There are only two attributes: velocity and position. Velocity represents the direction and distance of the next iteration, while position represents a solution to the problem. When PSO is initialized, all individuals in the flock forage in their own space. When the individuals find the food (the optimal solution of the problem), the solution is taken as the individual optimal solution ($P_{id,pbest}$); All the individual optimal solutions in the group are shared, and the quality of the solutions is evaluated by the fitness function to obtain the group optimal solution ($P_{d,gbest}$). In the next iteration, each individual updates its speed and position through the group optimal solution and continues foraging until a unique optimal solution is obtained [29]. The PSO algorithm flow is shown in Figure 4.
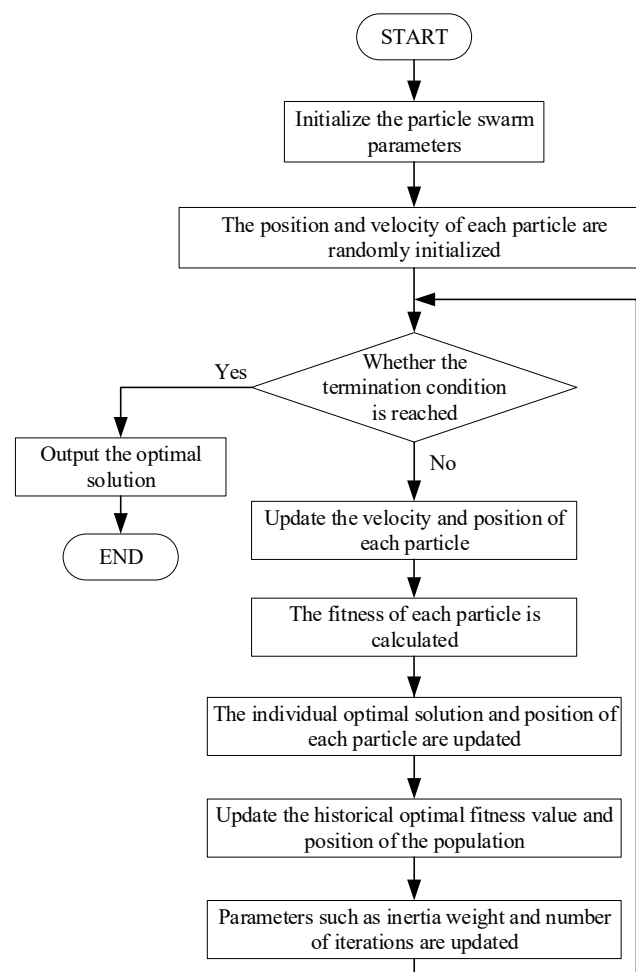

Figure 4. PSO algorithm flowchart.

Suppose there are N particles in the D–dimensional search space, and each particle represents a solution, then the position of the *i*th particle is $X_{id} = \{x_{i1}, x_{i2}, \ldots, x_{iD}\}$, the velocity of the *i*th particle is $V_{id} = \{v_{i1}, v_{i2}, \ldots, v_{iD}\}$, the optimal position searched by the *i*th particle (the individual optimal solution) is $P_{id,pbest} = \{p_{i1}, p_{i2}, \ldots, p_{iD}\}$, the optimal position searched by the group (the group optimal solution) is $P_{d,gbest} = \{p_{1,gbest}, p_{2,gbest}, \ldots, p_{D,gbest}\}$, and the individual historical optimal fitness value is f_p. The optimal population historical adaptation value is f_g. The algorithm is simple in structure, easy to implement, and has the advantages of high precision and short processing time.

Speed updating formula [29]:

$$v_{id}^{k+1} = wv_{id}^k + c_1 r_1 (P_{id,pbest}^k - x_{id}^k) + c_2 r_2 (P_{d,gbest}^k - x_{id}^k) \tag{7}$$

The location update formula is as follows [29]:

$$x_{id}^{k+1} = x_{id}^k + v_{id}^{k+1} \tag{8}$$

where *i* is the particle number, *d* is the particle dimension number, *k* is the number of iterations, *w* is the inertia weight, c_1 is the individual learning factor, c_2 is the group learning factor, and r_1 and r_2 are random numbers between 0 and 1. The velocity vector of particle *i* in the *d*-th dimension is the v_{id}^k in the *k*-th iteration. The position vector of particle *i* in the *d*-th dimension in the *k*-th iteration is the x_{id}^k. The historical optimal position of particle *i* in the *d*-th dimension in the *k*-th iteration is the $P_{id,pbest}^k$. The historical optimal position of the swarm in the *d*-th dimension in the *k*-th iteration is the $P_{d,gbest}^k$.

(2) LSTM model

The long short–term memory (LSTM) network model is composed of multiple repeated structural modules, and each structural module contains three gates: the forgetting gate, the input gate, and the output gate [30]. Figure 5 shows the LSTM model structure. The LSTM network realizes the control of three gates through the activation function so as to realize the retention and forgetting of historical information.
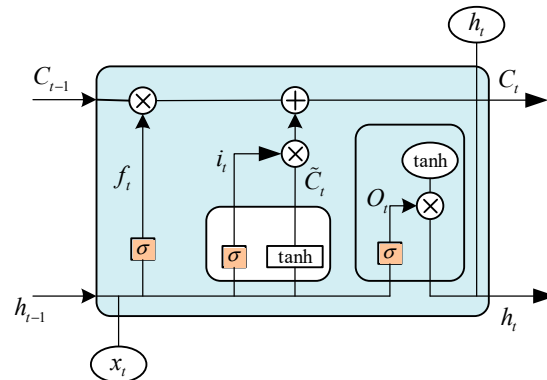

Figure 5. LSTM model structure diagram.

LSTM prediction model mainly includes three steps:

The forget gate f_t determined by the sigmoid function layer is calculated as follows:

$$f_t = \sigma(W_f[h_{t-1}, x_t] + b_f), \tag{9}$$

where, the sigmoid activation function is denoted by σ; The forgetting gate weight matrix is denoted by W_f; The neuron output is denoted by *h*; The neuron input is denoted by *x*; The current time is denoted by *t*. The previous time is denoted by $t-1$; The bias term is denoted by b_f.

The input gate to increase the amount of state is i_t, optionally updated. The calculation formula is shown in Equations (4)–(6):

$$i_t = \sigma(W_f[h_{t-1}, x_t] + b_i), \tag{10}$$

$$\widetilde{C}_t = \tanh(W_c[h_{t-1}, x_t] + b_c), \tag{11}$$

$$C_t = f_t C_{t-1} + i_t \widetilde{C}_t, \tag{12}$$

where, the alternative update information at time t is denoted by $\widetilde{C}_t$; The activation function is denoted by $\tanh()$. W_c represents the weight matrix of memory cells; C_t and C_{t-1} denote the memory cell state at time t and $t-1$, respectively.

The output gate is denoted by O_t and is calculated as follows:

$$O_t = \sigma(W_o[h_{t-1}, x_t] + b_o), \tag{13}$$

$$h_t = O_t \tanh C_t, \tag{14}$$

where, the output gate weight matrix is denoted by W_o.

3.2. Drilling 3D Model Construction Method

Python 3.7 is a major release of the Python programming language that introduces a number of new features and improvements that provide developers with a more powerful and flexible programming environment. The main characteristics of Python can be summarized as follows: it is simple and easy to learn, free source code, open source, and reduces the cost of learning; it has a wealth of high–quality libraries such as Pandas, Numpy, and Matplotlib that provide powerful support for data processing, computation, and plotting.

When generating the 3D model, the 3D coordinates of the reference point are determined, and the coordinates of the other vertices are calculated by the 3D spatial relationship between the other vertices of the model and the reference point. The scatter() function in Python was used to generate each vertex, and the wiring function was used to connect the relevant vertices according to the model design to generate the model contour. Then, the surface function is used to connect the contour lines in turn to form the model section and finally generate the three–dimensional space model. Figure 6 shows the rapid generation process of the 3D spatial model of the borehole.
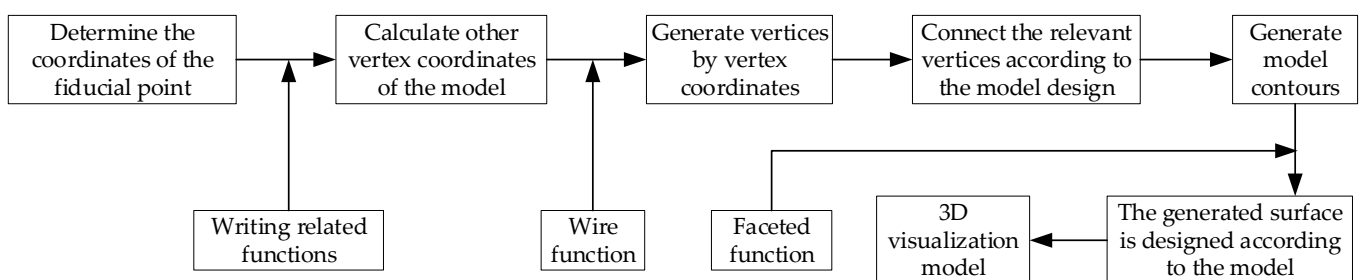
Figure 6. Flowchart of rapid generation of 3D space model for drilling.

3.3. Specific Implementation Ideas

In order to realize the intelligent optimization of gas drilling parameters and the rapid generation of a three–dimensional space model based on big data mining technology, Python programming language, and MATLAB R2021b programming language are used to construct the intelligent optimization model of drilling parameters and the rapid generation algorithm of the three–dimensional space model. Specific research steps are as follows: in the process of borehole design, firstly, the regional gas extraction conditions are analyzed, and according to the gas extraction law knowledge in the knowledge base, the gas extraction law of the extraction region is determined. Then, according to the law of gas extraction and the allowable time of gas pre–extraction, the spacing of the gas extraction holes at

various points is determined. Then, according to the occurrence of the coal seam, the position of the drilling hole was determined by fully considering the performance of the drilling machine and drilling tool, and the azimuth Angle, dip Angle, and hole depth of each drilling hole were calculated by the spatial geometry method. Finally, according to the drilling design parameters, a drilling design map is automatically drawn to complete the intelligent drilling design. Its flowchart is shown in Figure 7.

1. Analysis of influencing factors of effective extraction radius: From the perspective of the theoretical formula of effective extraction radius, the influencing factors are analyzed. The factors that can be effectively controlled in the actual production process include extraction time, hole diameter, hole spacing, and extraction negative pressure. Therefore, numerical simulation software is used to construct geometric models and divide grids, and the gas pressure changes under different parameters are studied from these four aspects.

2. Intelligent optimization model of drilling parameters: in order to find more suitable drilling parameters, big data mining technology is used to learn the drilling experience of successful cases, and the long short–term memory neural network model of particle swarm optimization is constructed by MATLAB to determine the key parameters of the model and optimize the drilling parameters of gas extraction.

3. 3D space model generation algorithm: The Python open–source program is used as the compilation language, and the modeling idea of "generating lines from points, lines from surfaces, and surfaces from surfaces" is used to generate the corresponding 3D space model with the optimized parameters in step 2.
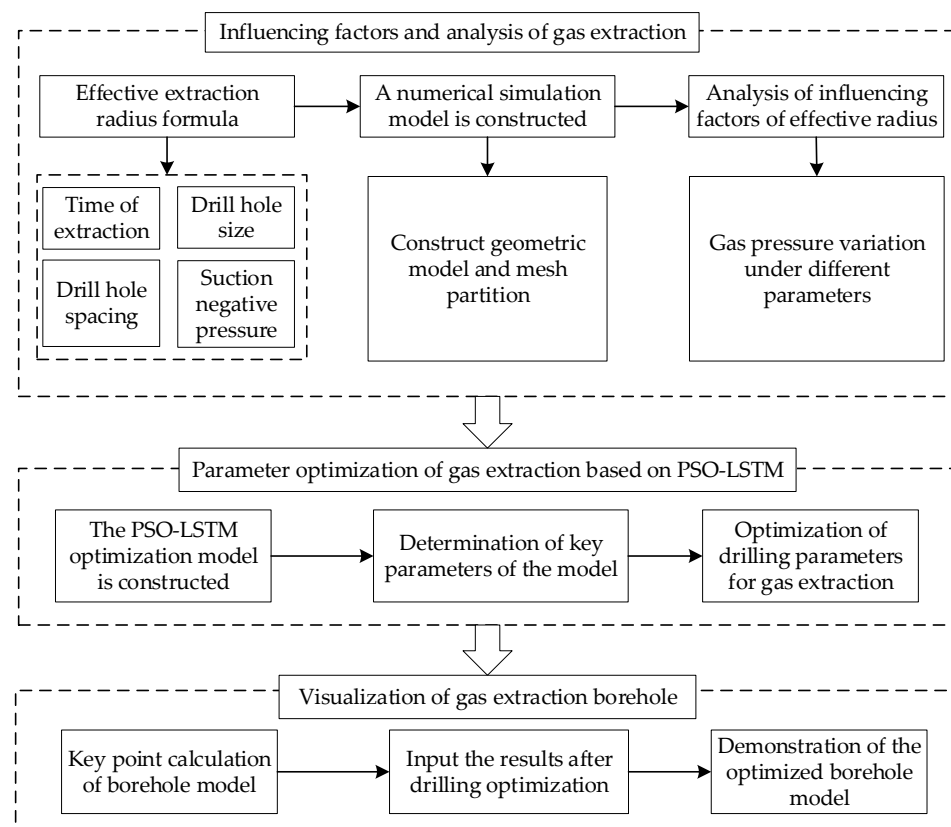

Figure 7. Basic Implementation Idea.

4. Parameter Optimization Method of Gas Extraction Based on PSO–LSTM

The design of a drilling hole is the main basis of drilling construction. The scientific and rational design of drilling holes directly affects the difficulty of drilling construction and the amount of engineering, as well as the play of later extraction efficiency. The

design of extraction drilling must be considered from various factors. It is a complex decision–making process that is limited by various factors such as coal seam gas geological conditions, drilling construction environment, drilling machine drilling tool performance and so on. It needs to balance various needs, such as gas extraction standards, drilling construction difficulty, drilling amount and so on, so that the drilling layout scheme can achieve the overall optimization state. To solve this black–box problem, it is an effective way to construct a long short–term memory neural network model based on particle swarm optimization. The model can fuse coal mine geological data, gas monitoring data, and other related information and realize transparent and intelligent analysis of gas geological conditions.

4.1. Optimization Model Construction

Particle Swarm Optimization long short–term memory neural network model (PSO–LSTM) is a combination of Particle swarm optimization (PSO) and long short–term memory (LSTM). (LSTM) performs double training on gas drilling data and uses the optimization results of the PSO algorithm as the test set of the LSTM algorithm, which makes the training results of the LSTM algorithm more accurate [31], and the flow chart is shown in Figure 8.
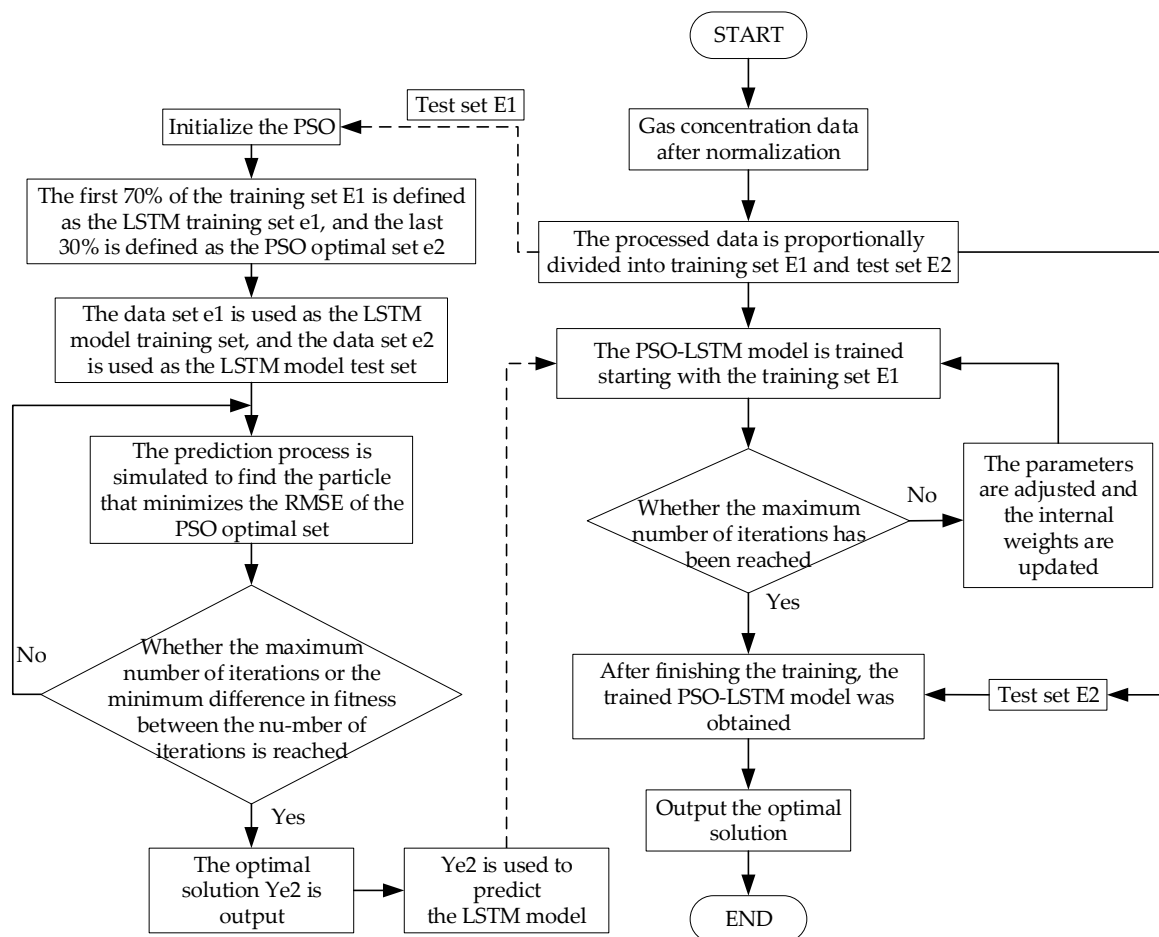
Figure 8. Flowchart of the PSO–LSTM model.

The specific process is as follows:

Step 1: The gas drilling data Xn is standardized according to the format so that it conforms to the data processing flow; The processed data is divided into training set E_1 and test set E_2 in proportion. In equations Xn, E_1, and E_2, R_i is the drilling radius, di is the drilling spacing, and $i = \{1, 2, \ldots, n\}$.

Step 2: Start with the training set E1 and the PSO model to optimize and train the LSTM model. The specific process is as follows:

(1) The PSO algorithm is initialized to form an optimization community.

(2) The conventional prediction model divides the training set and the test set according to a ratio of 7:3. Therefore, the first 70% of the training set E_1 is defined as the LSTM model training set $e1 = (\sum_i^n R_i, \sum_i^n d_i)$, and the last 30% is defined as the PSO model optimization set $e2 = (\sum_i^n R_i, \sum_i^n d_i)$.

(3) The LSTM model training set e1 is used as the training set of the LSTM model, and the optimal solution of the PSO model optimization set e2 is used as the test set of the LSTM model.

(4) Start the simulation prediction process to find the particle that minimizes the RMSE of the PSO selection set (training result). Meanwhile, the training set e1 is used to train the LSTM model.

Root Mean Square Error (RMSE) is used as the evaluation index to detect whether the PSO model training reaches the maximum number of iterations or the minimum difference in fitness between iterations.

$$RMSE = \sqrt{\frac{\sum_{i=1}^{n} (X_{obs,i} - X_{pre,i})^2}{n}} \tag{15}$$

(5) Output the optimal solution $Y_{e2} = (\sum_i^n R_i, \sum_i^n d_i)$ of optimal set e2 of PSO model, $i = \{1, 2, \ldots, n\}$.

Step 3: Use the optimal solution $Y_{e2} = (\sum_i^n R_i, \sum_i^n d_i)$ of the PSO model selection e2 to predict and analyze the LSTM model that has been trained.

Step 4: Adjust the model parameters based on the predictions. If it does not, the parameters are adjusted, the internal weights are updated, and the PSO–LSTM model is returned for training again until the training result reaches the maximum number of iterations.

Step 5: After the training of the PSO–LSTM model, the test set E2 is used to predict and analyze the trained PSO–LSTM model.

Step 6: Output the PSO–LSTM model optimal solution $Y_n = (\sum_i^n R_i, \sum_i^n d_i)$, $i = \{1, 2, \ldots, n\}$.

4.2. Determination of Key Parameters

When constructing the PSO–LSTM model, it is necessary to consider how to establish its key parameters and the influence of the data itself on the prediction accuracy so as to improve the performance of the model by reasonably establishing these parameters. The parameters of the PSO algorithm were as follows: the number of the initial populations was five, the dimension of the initial population was two, the maximum iteration number of the initial population was 10, the learning factor $c_1 = c_2 = 2$, the maximum inertia weight was 1.2, and the minimum inertia weight was 0.8. The parameters of the PSO–LSTM model are input layer dimension 2, output layer dimension 1, hidden layer neuron number 10~200, learning rate 0.01~0.15, iteration number 50, and stochastic gradient descent algorithm [32]. The key parameters are shown in Table 2.

PSO Algorithm Parameter		PSO–LSTM Algorithm Parameter	
Parameter	Parameter Value	Parameter	Parameter Value
Initialize the number of groups	5	Input layer dimension	2
Initialize the group dimensions	2	Output layer dimension	1
Initialize the maximum number of swarm iterations	10	Number of neurons in the hidden layer	10~200
Learning factor c_1	2	LSTM layer	PSO optimization
Learning factor c_2	2	solver	Adam
Maximum inertia weight	1.2	Learning rate	Adaptive
Minimum inertia weight	0.8	Number of iterations	50

5. Fast Generation Algorithm for 3D Borehole Model

According to the above–optimized drilling parameters and 3D coordinate information of coal seam, the rapid generation algorithm of 3D drilling space is realized based on the modeling idea of "generating lines from points, generating surfaces from lines, and generating bodies from surfaces". It consists of two parts: the 3D model generation of bedding drilling and through drilling. Generate 3D models of boreholes covering necessary parts such as coal seams, laneways, and boreholes.

5.1. Key Point Calculation of Bedding Borehole Model

The 3D modeling of the working face is carried out by using the drilling of bedding on both sides of the strike. In the ideal state, the 3D drilling model of the inlet roadway and the return roadway is shown in Figure 9, in which the starting and ending coordinates of the intersection line between the working face and the bottom of the inlet roadway are $A_1(x_{A_1}, y_{A_1}, z_{A_1})$ and $B_1(x_{B_1}, y_{B_1}, z_{B_1})$ respectively, and the starting and ending coordinates of the intersection line between the working face and the bottom of the return roadway are $C_1(x_{C_1}, y_{C_1}, z_{C_1})$ and $D_1(x_{D_1}, y_{D_1}, z_{D_1})$ respectively. The length along coal seam strike is L_{Z1}, the slant width of working face is L_{W1}, the azimuth Angle of the roadway is α_1, the Angle between coal seam strike and horizontal plane is β_1, the azimuth Angle of drill hole in inlet roadway is θ_1, and the azimuth Angle of the drill hole in return roadway is θ_2. A schematic diagram of the drill hole arrangement of the k unit is shown in Figure 10.
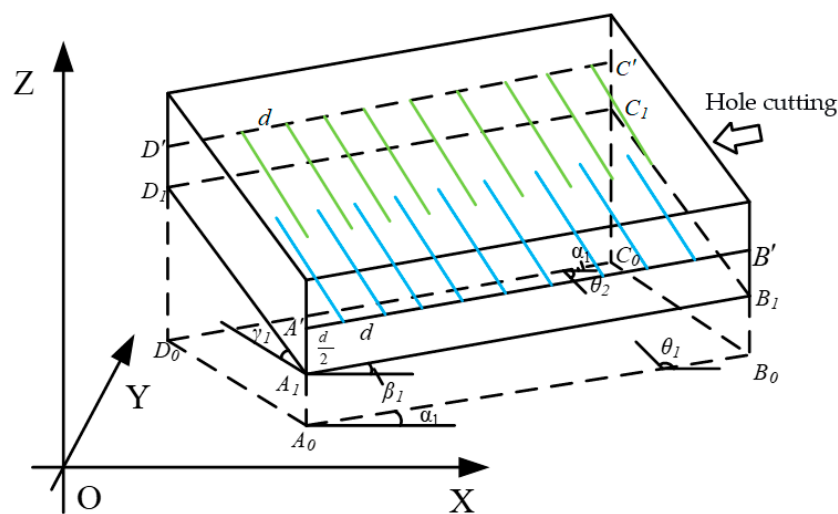

Figure 9. Schematic diagram of the 3D model of drilling in counterpunching bedding.
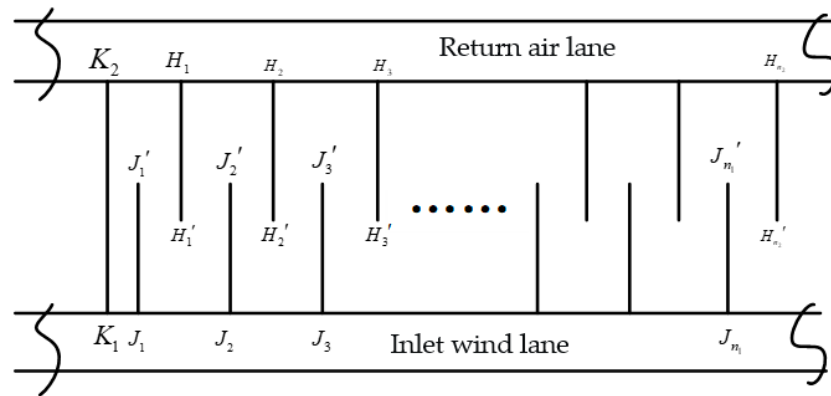
Figure 10. Diagram of drill hole arrangement in unit k.

The coordinate of the control point of the first unit of the inlet wind lane is $(x_{A_1}, y_{A_1}, z_{A_1} + \frac{L_h}{2})$.

(1) Coordinates of inlet lane

The coordinate of the n_1 opening point of the KTH element is $J_{n_1}(x_{J_{n_1}}, y_{J_{n_1}}, z_{J_{n_1}})$:

$$
\begin{cases}
x_{J_{n_1}} = x_{A_1} + \sum_1^{k-1} L_k \cos(\beta_1)\cos(\alpha_1) + (n_1 - \frac{1}{2})d_k \cos(\beta_1)\cos(\alpha_1) \\[2mm]
y_{J_{n_1}} = y_{A_1} + \sum_1^{k-1} L_k \cos(\beta_1)\sin(\alpha_1) + (n_1 - \frac{1}{2})d_k \cos(\beta_1)\sin(\alpha_1) \\[2mm]
z_{J_{n_1}} = z_{A_1} + \frac{L_h}{2} + \sum_1^{k-1} L_k \sin(\beta_1) + (n_1 - \frac{1}{2})d_k \sin(\beta_1)
\end{cases}
\tag{16}
$$

where, n_1 represents the number of pumping holes in the inlet lane of unit k.

The coordinate of the n_1 final hole point of the KTH element is $J'_{n_1}(x_{J'_{n_1}}, y_{J'_{n_1}}, z_{J'_{n_1}})$:

$$
\begin{cases}
x_{J'_{n_1}} = x_{A_1} + \sum_1^{k-1} L_k \cos(\beta_1)\cos(\alpha_1) + (n_1 - \frac{1}{2})d_k \cos(\beta_1)\cos(\alpha_1) - L_c \cos(\gamma_1)\sin(\alpha_1) \\[2mm]
y_{J'_{n_1}} = y_{A_1} + \sum_1^{k-1} L_k \cos(\beta_1)\sin(\alpha_1) + (n_1 - \frac{1}{2})d_k \cos(\beta_1)\sin(\alpha_1) + L_c \cos(\gamma_1)\cos(\alpha_1) \\[2mm]
z_{J'_{n_1}} = z_{A_1} + \frac{L_h}{2} + \sum_1^{k-1} L_k \sin(\beta_1) + (n_1 - \frac{1}{2})d_k \sin(\beta_1) + L_c \sin(\gamma_1)
\end{cases}
\tag{17}
$$

where, $\frac{L_h}{2}$ represents the distance between coal seam A_1 and $A_1{'}$, m; γ is the dip Angle of coal seam, °; L_c is the length of the extraction drilling hole, m, $L_c \geq L_w/2 + 5$.

(2) Return air lane

The coordinate of the n_2 opening point of the KTH element is $H_{n_2}(x_{H_{n_2}}, y_{H_{n_2}}, z_{H_{n_2}})$:

$$
\begin{cases}
x_{H_{n_2}} = x_{A_1} - L_{w1} \cos(\gamma_1)\sin(\alpha_1) + \sum_1^{k-1} L_k \cos(\beta_1)\sin(\alpha_1) + n_2 d_k \cos(\beta_1)\cos(\alpha_1) \\[2mm]
y_{H_{n_2}} = y_{A_1} + L_{w1} \cos(\gamma_1)\cos(\alpha_1) + \sum_1^{k-1} L_k \cos(\beta_1)\cos(\alpha_1) + n_2 d_k \cos(\beta_1)\sin(\alpha_1) \\[2mm]
z_{H_{n_2}} = z_{A_1} + \frac{L_h}{2} + L_{w1} \sin(\gamma_1) + \sum_1^{k-1} L_k \sin(\beta_1) + n_2 d_k \sin(\beta_1)
\end{cases}
\tag{18}
$$

The coordinate of the n_2 final hole point of the KTH element is $H'_{n_2}(x_{H'_{n_2}}, y_{H'_{n_2}}, z_{H'_{n_2}})$:

$$
\begin{cases}
x_{H'_{n_2}} = x_{A_1} - L_{w1} \cos(\gamma_1)\sin(\alpha_1) + \sum_1^{k-1} L_k \cos(\beta_1)\sin(\alpha_1) + n_2 d_k \cos(\beta_1)\cos(\alpha_1) + L_c \cos(\gamma_1)\sin(\alpha_1) \\[2mm]
y_{H'_{n_2}} = y_{A_1} + L_{w1} \cos(\gamma_1)\cos(\alpha_1) + \sum_1^{k-1} L_k \cos(\beta_1)\cos(\alpha_1) + n_2 d_k \cos(\beta_1)\sin(\alpha_1) - L_c \cos(\gamma_1)\cos(\alpha_1) \\[2mm]
z_{H'_{n_2}} = z_{A_1} + \frac{L_h}{2} + L_{w1} \sin(\gamma_1) + \sum_1^{k-1} L_k \sin(\beta_1) + n_2 d_k \sin(\beta_1) - L_c \sin(\gamma_1)
\end{cases}
\tag{19}
$$

where, n_2 represents the number of drilling holes in the return air lane of unit k.

5.2. Key Point Calculation of Through–Layer Drilling Model

A schematic diagram of the 3D model of through–layer drilling is shown in Figure 11, which is composed of four parts: the bottom coal pumping roadway with $A_2B_2C_2D_2$ as the top surface, the pre–pumping coal seam with $A_3B_3C_3D_3$ as the bottom surface, the pre–driving coal roadway with $A_4B_4C_4D_4$ as the bottom surface, and the red and blue drilling trajectories. It is assumed that the inclination angles of the bottom pumping roadway, the pre–pumping coal seam and the pre–tunneling coal roadway are the same, and the bottom pumping roadway is $A_2(x_{A_2}, y_{A_2}, z_{A_2})$, $B_2(x_{B_2}, y_{B_2}, z_{B_2})$, $C_2(x_{C_2}, y_{C_2}, z_{C_2})$ and $D_2(x_{D_2}, y_{D_2}, z_{D_2})$. Pre–pumped coal seam $A_3(x_{A_3}, y_{A_3}, z_{A_3})$, $B_3(x_{B_3}, y_{B_3}, z_{B_3})$, $C_3(x_{C_3}, y_{C_3}, z_{C_3})$, $D_3(x_{D_3}, y_{D_3}, z_{D_3})$; Coal roadway $A_4(x_{A_4}, y_{A_4}, z_{A_4})$, $B_4(x_{B_4}, y_{B_4}, z_{B_4})$, $C_4(x_{C_4}, y_{C_4}, z_{C_4})$ and $D_4(x_{D_4}, y_{D_4}, z_{D_4})$ were pre–tunneled. The length along the strike of the coal seam is L_{Z2}, the slant width of the working face is L_{W2}, the azimuth Angle of the roadway is α_2, and the Angle between the strike of the coal seam and the horizontal plane is β_2.
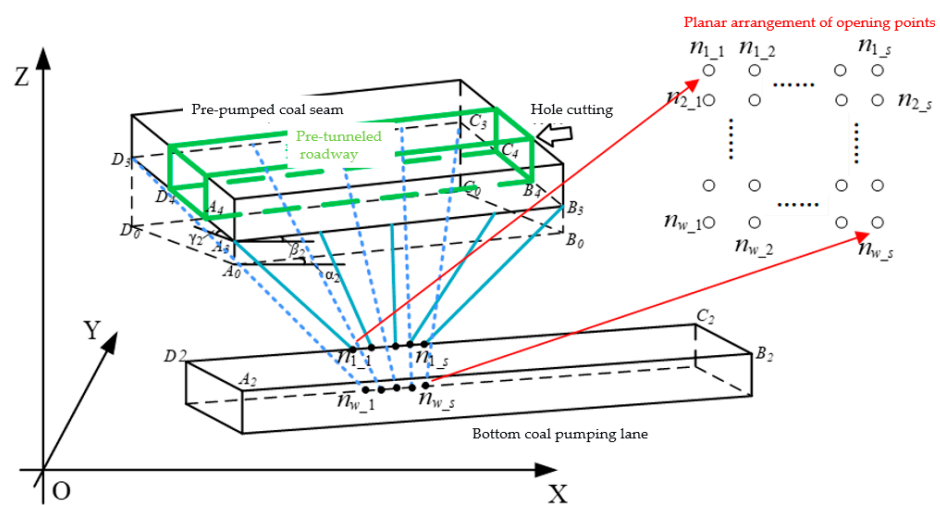

Figure 11. Schematic diagram of 3D model of through–layer drilling hole.

The planar diagram of the opening point is similar to that of the final hole point, as shown in "Opening point planar Arrangement" in Figure 11, where n_{w_s} represents the s-th drilled hole in the w row. The difference is that the opening point is located at the back side of the bottom extraction roadway, and the final hole point is located at the bottom of the pre–extraction seam.

(1) Coordinates of opening points

The s opening point in row w is $K_{n_{w\_s}}(x_{K_{n_{w\_s}}}, y_{K_{n_{w\_s}}}, z_{K_{n_{w\_s}}})$:

$$
\begin{cases}
x_{K_{n_{w\_s}}} = x_{D_2} + K_{d_0}\cos(\beta_2)\cos(\alpha_2) + \sum_1^{s-1} K_{d_1}\cos(\beta_2)\cos(\alpha_2) + \sum_1^{s-1} K_{d_1}\cos(\beta_2)\cos(\alpha_2) \\
y_{K_{n_{w\_s}}} = y_{D_2} + K_{d_0}\cos(\beta_2)\sin(\alpha_2) + \sum_1^{s-1} K_{d_1}\cos(\beta_2)\sin(\alpha_2) + \sum_1^{s-1} K_{d_1}\cos(\beta_2)\sin(\alpha_2) \\
z_{K_{n_{w\_s}}} = z_{D_2} + K_{d_0}\sin(\beta_2) + \sum_1^{s-1} K_{d_1}\sin(\beta_2) - \sum_1^{w-1} K_{d_2}\sin(\beta_2)
\end{cases}
\tag{20}
$$

where, K_{d0} represents the distance between $K_{n_{1\_1}}$ and D_2 point, m; K_{d1} represents the spacing of the opening point column, m; K_{d2} denotes the row spacing of the opening points, m.

(2) Final hole point coordinates

The s-th final hole point in row w is $Z_{n_{w\_s}}(x_{Z_{n_{w\_s}}}, y_{Z_{n_{w\_s}}}, z_{Z_{n_{w\_s}}})$:

$$
\begin{cases}
x_{Z_{n_{w\_s}}} = x_{A_3} + \sum_1^{s-1} Z_{d_1}\cos(\beta_2)\cos(\alpha_2) - \sum_1^{w-1} Z_{d_2}\cos(\beta_2)\sin(\alpha_2) \\
y_{Z_{n_{w\_s}}} = y_{A_3} + \sum_1^{s-1} Z_{d_1}\cos(\beta_2)\sin(\alpha_2) + \sum_1^{w-1} Z_{d_2}\cos(\beta_2)\cos(\alpha_2) \\
z_{Z_{n_{w\_s}}} = z_{A_3} + \sum_1^{s-1} Z_{d_1}\sin(\beta_2) + \sum_1^{w-1} Z_{d_2}\sin(\gamma_2)
\end{cases}
\tag{21}
$$

where, Z_{d1} represents the spacing of the final hole point column, m; Z_{d2} represents the row spacing of the terminal hole point, m.

6. Application Example and Effect Evaluation

6.1. Source of Cases

The test site was selected as the 1302 working face of a coal mine in Shanxi Province, with a coal seam thickness of 5.3 m and a coal seam dip Angle of 16°. There are two grooves in the working face, and there is a high extraction roadway below the coal seam. According to the actual demand of the mine, gas extraction work is carried out from two laneways, including gas extraction work of low through–layer drilling and gas extraction work of bedding drilling. Considering the complexity, time–consuming, and labor–intensive manual design of gas extraction drilling, a method of artificial intelligence is proposed to quickly design the parameters of gas extraction drilling, and the visual display of the gas extraction drilling field is realized by means of software programming.

6.2. Case 1 Result Analysis (Bedding Extraction)

(1) Optimization of drilling parameters

Based on the extraction records of the adjacent working face, 30 historical data points of the drilling holes along the layer were selected to verify the effectiveness of the above method, in which the diameter of the drilling holes along the layer was not less than 94 mm. The first 24 (80%) of each group of data were used as the training set, and the PSO–LSTM model was used to optimize and train the drilling parameters. The last six items (20%) were used as the test set to predict the optimization results. Among them, the first 17 (70%) items of the test set were used as the LSTM model training set, and the last seven (30%) items were used as the PSO model optimization set.

By defining the size, iteration number, inertia weight, acceleration coefficient, and other parameters of the particle swarm, the particle swarm is initialized, and the LSTM network structure is designed, including the input layer, hidden layer, and output layer, and relevant parameters such as the time step and the number of hidden layer units are set. PSO was combined with LSTM, the initial weights and hyperparameters of LSTM were optimized by PSO, and the model was trained until it converged to the optimal solution as shown in Table 3.

**Table 3.** Comparison of drilling parameter optimization results in bedding.

Serial Number	Data Types	Drill Hole Spacing/(m)	Drill Hole Depth/(m)	Inclination of Drill Hole/(°)	Borehole Azimuth/(°)
X1	Training set	9.1	28.7	18.17	29.87
X2	Training set	8.4	29.5	16.92	29.26
X3	Training set	8.8	30.0	17.91	30.08
		. . . . . .			
T1	Test set	8.1	29.7	17.30	30.21
T2	Test set	8.3	28.7	17.11	30.15
T3	Test set	8.2	30.1	16.81	29.72
		. . . . . .			
Y1	Design results	6	30.0	16.00	30.00

Table 3 shows that the drilling parameters designed using the PSO–LSTM optimization model are spacing 6 m, drilling hole depth 30 m, drilling dip Angle 16°, and azimuth Angle 30°. The design results are the same as the drilling parameters designed using numerical simulation, and the time consumption is shorter, which shows the accuracy and convenience of the method.

(2) Visual display of drill field

The design results in Table 3 are incorporated into the compiled drill–field visualization model, and the results are shown in Figure 12. It can be seen from Figure 12 that the drill

holes of the inlet and return air roadways are different, and the length of the drill holes is greater than half of the width of the extracted coal seam. This method of hole distribution can fully extract coal seam gas and avoid an excessive concentration of residual gas. The drill holes of the inlet lane and return lane are numbered. There are 25 drill holes in the inlet lane (lower side) and 24 drill holes in the return lane (upper side).

(a)

(b)

(c)
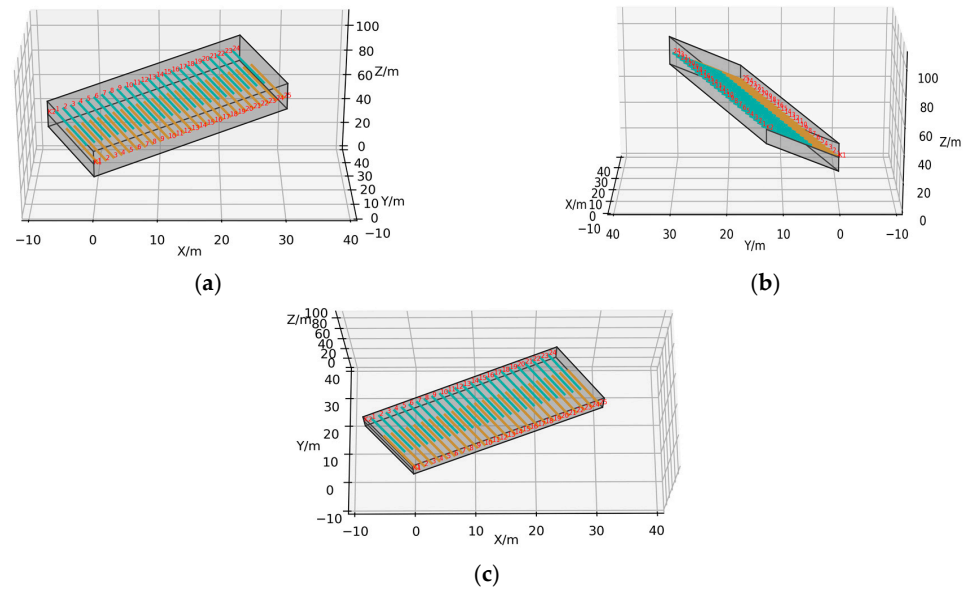
Figure 12. Renderings of 3D model of bedding borehole. (**a**) Main view; (**b**) Left view; (**c**) Top view.

6.3. Case 2 Result Analysis (Through–Layer Extraction)

3D visualization of the through–layer drilling holes is shown in Figure 13. There are 72 through–layer drilling holes (nine rows and eight columns), and the opening points and final hole points of the drilling holes are arranged neatly and numbered from 1 to 72. Figure 13c shows that the effective extraction range of the final hole point of each drilling hole overlaps with each other and is tightly connected, covering the whole pre–extracted coal seam, which can fully extract coal seam gas. Due to space limitations, the optimization process of through–layer drilling will not be described again.

(a)

(b)

(c)
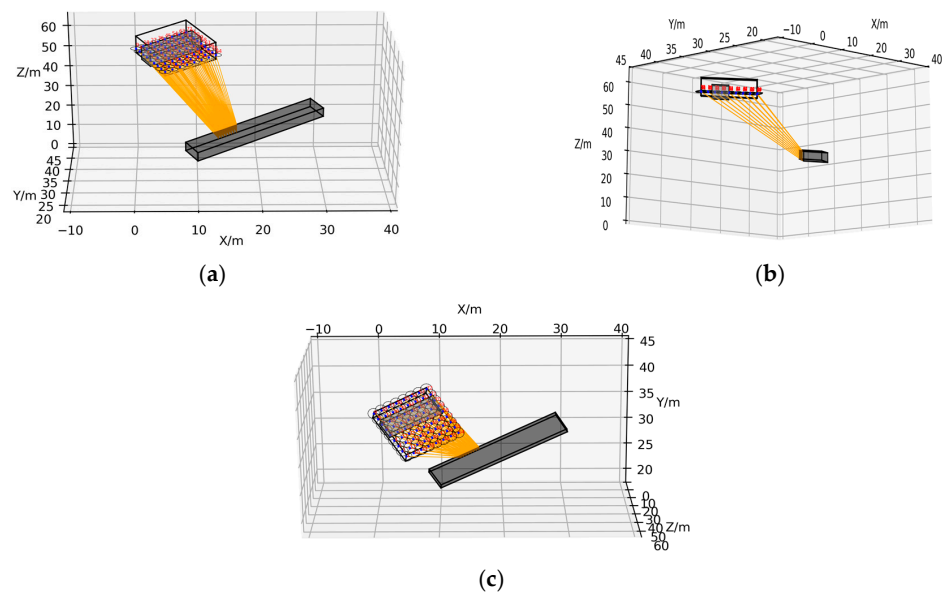
Figure 13. 3D visualization rendering of through–layer drilling. (**a**) Main view; (**b**) Left view; (**c**) Top view.

6.4. Discussion

With the gradual development of intelligent construction in mines, it is imperative to automate and intelligentize gas extraction. Based on this, this study proposes an intelligent optimization method based on PSO–LSTM and combines 3D visualization technology to carry out intelligent design and visual display research of extraction drilling parameters, which improves the scientific and intuitive design of gas extraction drilling and provides strong support for coal mine safety production. Through a later test, the above method is used to realize the rapid design of gas extraction parameters, drilling concentration, negative pressure, and other composite–related requirements. At the same time, the generation of a three–dimensional drilling field lays the foundation for the visual display of the gas extraction drilling field and ensures the safe and efficient recovery of the working face.

Gas extraction is a "four–dimensional" dynamic process, which needs to fully consider the dimensions of space and time. Differential borehole parameter design is an indispensable problem in gas extraction, and gas transparent geology technology is a key link. In order to improve the accuracy and timeliness of geological condition detection and coal seam gas measurement, advanced coal seam geological detection and coal seam gas parameter measurement techniques are studied for dynamic transparent gas geology. Establishing a GIS–based gas geological information platform, constructing a high–precision three–dimensional gas geological dynamic model, and accurately, intuitively, and dynamically displaying the gas geological conditions and their evolution process in the whole life cycle of gas extraction are the main development trends of gas geological security in intelligent gas extraction.

In the future, based on the above theoretical research, the team will further develop the automatic design platform of gas extraction drilling, improve the functions of extraction drilling design, 3D model generation, drawing output, and so on, and form a full–cycle control platform of "design–construction–acceptance –observation –enrichment –abandonment" of gas extraction drilling. It integrates the functions of auxiliary analysis of borehole spacing, automatic calculation of borehole parameters, automatic drawing of design drawings, three–dimensional display of design effects, etc., and realizes the automatic design of boreholes for common types of gas extraction in coal mines, such as through layers, along layers, and high positions. At the same time, it is further explored to combine other optimization algorithms with deep learning models to improve the intelligence level of drilling design and expand its application in other mine safety production fields.

7. Conclusions

Aiming at the problems of low utilization rate of gas extraction parameters and long design cycle of the gas extraction scheme, an intelligent design and visualization method of gas extraction drilling based on PSO–LSTM was proposed. The PSO–LSTM model uses the PSO algorithm to optimize the parameters of the LSTM model and search for the most suitable LSTM model parameters to improve the accuracy of the LSTM algorithm.

1. From the perspective of the theoretical formula of extraction radius, the law of extraction radius with different drilling parameters is studied; that is, the extraction range increases with the increase in extraction time, drilling diameter, and extraction negative pressure. Within a certain range, the extraction range increases with an increase in borehole spacing, which provides a theoretical basis for the intelligent optimization of extraction parameters.
2. This paper proposes an intelligent optimization method for gas extraction drilling parameters based on depth mining. Using the experience of successful cases of gas extraction drilling in–depth mining by this method, taking the successful actual parameters as a reference, intelligent optimization of 1302 working face drilling parameters: drilling spacing 6 m, drilling depth 30 m, drilling Angle 16°, azimuth Angle 30°, improve the accuracy of the model.
3. The mathematical expressions of the gas extraction space models for the bedding and through–layer boreholes are summarized. Based on the modeling idea of the point–

generating line, line–generating surface, and surface–generating body", through the intelligent optimization of drilling parameters and 3D coordinate information of the coal seam, a 3D space model of bedding and throughbed is generated. This method uses a Python open–source program as the basic modeling language, which overcomes the shortcomings of other modeling software with diverse operations and complexity. In addition, Python can automate the modeling process by writing scripts, reducing manual time and errors. This is particularly important for scenarios in which fast iterations are required, or a large number of models need to be processed.

4. Taking the 1302 working face of a coal mine in Shanxi Province as the research object, the drilling parameters are designed by numerical simulation and the PSO–LSTM model. The research in Section 5.2 shows that the drilling parameters designed by numerical simulation and the PSO–LSTM model are similar, which verifies the accuracy of the PSO–LSTM model and provides some support for the intelligent mining of coal mines.

References

1. Wang, P.; Ni, H.; Wang, R.; Li, Z. Modulating downhole cuttings via a pulsed jet for efficient drilling–tool development and field testing. *J. Nat. Gas Sci. Eng.* **2015**, *27*, 1287–1295. [CrossRef]
2. Xue, Y.; Liu, J.; Ranjith, P.; Liang, X.; Wang, S. Investigation of the influence of gas fracturing on fracturing characteristics of coal mass and gas extraction efficiency based on a multi–physical field model. *J. Pet. Sci. Eng.* **2021**, *206*, 109018. [CrossRef]
3. Pan, H. Optimized design of gas extraction parameters by high–positioned drill–holes. *China Coal* **2009**, *35*, 106–107+115.
4. Li, T.; Wu, B.; Lei, B. Study on the optimization of a gas drainage borehole drainage horizon based on the evolution characteristics of mining fracture. *Energies* **2019**, *12*, 4499. [CrossRef]
5. Yan, Z.; Wang, Y.; Fan, J.; Huang, Y.; He, Y. Study on Key Parameters of Directional Long Borehole Layout in High–Gas Working Face. *Shock Vib.* **2021**, *2021*, 5579967. [CrossRef]
6. Huang, Y. Optimization study of hydraulic slotting parameters for soft coal seam in Yuwu Coal Mine. *Min. Saf. Environ. Prot.* **2022**, *49*, 61–65.
7. Wu, K.; Shi, S.; Lu, Y.; Li, H.; Li, M. Optimization of the Plastic Area of a Borehole Based on the Gas Extraction Effect and Its Engineering Application. *Geofluids* **2021**, *2021*, 8147366. [CrossRef]
8. Yang, X.; Wen, G.; Lu, T.; Wang, B.; Li, X.; Cao, J.; Lv, G.; Yuan, G. Optimization and field application of CO_2 gas fracturing technique for enhancing CBM extraction. *Nat. Resour. Res.* **2020**, *29*, 1875–1896. [CrossRef]
9. Wang, Y.; Zhang, Y. Study on optimization of layout parameters of high–level boreholes in Pingdingshan coal mine. *Sci. Rep.* **2023**, *13*, 19759. [CrossRef]

10. Jing, G.; Wang, Y.; Zhou, F.; Tan, Z. Numerical Simulation Study of Water Fracturing with Different Angle through Beds Holes Based on RFPA2D. *Coal Min. Technol.* **2018**, *23*, 103–107.

11. Lin, H.; Ji, P.; Kong, X.; Li, S.; Dou, G.; Li, K. Precise borehole placement model and engineering practice for pre–draining coal seam gas by drilling along seam. *J. China Coal Soc.* **2022**, *47*, 1220–1234.

12. Luo, M.; Yang, L.; Wen, H.; Zhao, D.; Wang, K. Numerical Optimization of Drilling Parameters for Gas Predrainage and Excavating–Drainage Collaboration on Roadway Head. *Geofluids* **2022**, *2022*, 3241211. [CrossRef]

13. Lee, B.Y.; Liu, H.S.; Tarng, Y.S. Modeling and optimization of drilling process. *J. Mater. Process. Technol.* **1998**, *74*, 149–157. [CrossRef]

14. Lipin, K.; Govindan, P. A review on multi objective optimization of drilling parameters using Taguchi methods. *AKGEC Int. J. Technol.* **2013**, *4*, 11–21.

15. Zhao, Y.; Noorbakhsh, A.; Koopialipoor, M.; Azizi, A.; Tahir, M.M. A new methodology for optimization and prediction of rate of penetration during drilling operations. *Eng. Comput.* **2020**, *36*, 587–595. [CrossRef]

16. Ashena, R.; Rabiei, M.; Rasouli, V.; Mohammadi, A.H.; Mishani, S. Drilling parameters optimization using an innovative artificial intelligence model. *J. Energy Resour. Technol.* **2021**, *143*, 052110. [CrossRef]

17. Xie, B.; Zhong, S.; Cao, X. Automatic optimization design and application of drilling parameters for gas drainage in cross cut coal uncovering. *J. Min. Sci. Technol.* **2021**, *6*, 678–687.

18. Qin, Z.; Shen, H.; Yuan, Y.; Gong, Z.; Chen, Z.; Xia, Y. Determination of Gas Extraction Borehole Parameters in Fractured Zone on 'Borehole in Place of Roadway'Based on RSM–GRA–GA. *Processes* **2022**, *10*, 1421. [CrossRef]

19. Ding, Y.; Zhu, B.; Li, S.; Lin, H.; Wei, Z.; Li, L.; Long, H.; Yi, Y. Accurate identification and efficient drainage of relieved methane in goaf of high outburst mine. *J. China Coal Soc.* **2021**, *46*, 3565–3577.

20. Zhao, P.; Kang, X.; Li, S.; Lin, H.; Gan, L.; An, X. Optimization of "hole–drift" collaborative drainage layout parameters and high efficient drainage in pressure relief gas migration area. *Coal Sci. Technol.* **2022**, *50*, 137–146.

21. Shi, Z.; Ye, D.; Hao, J.; Qin, B.; Li, G. Research on gas extraction and cut flow technology for lower slice pressure relief gas under slice mining of extra-thick coal seam. *ACS Omega* **2022**, *7*, 24531–24550. [CrossRef]

22. Xie, Z.; Zhang, D.; Song, Z.; Li, M.; Liu, C.; Sun, D. Optimization of Drilling Layouts Based on Controlled Presplitting Blasting through Strata for Gas Drainage in Coal Roadway Strips. *Energies* **2017**, *10*, 1228. [CrossRef]

23. Yi, M.; Wang, L.; Hao, C.; Liu, Q.; Wang, Z. Method for designing the optimal sealing depth in methane drainage boreholes to realize efficient drainage. *Int. J. Coal Sci. Technol.* **2021**, *8*, 1400–1410. [CrossRef]

24. Xu, X.; Meng, X.; Zhao, G.; Wang, X.; He, Y. Virtual simulation of gas drainage drilling through layers in stress–relaxation zone based on three–dimensional visualization. *J. Saf. Sci. Technol.* **2014**, *10*, 77–82.

25. Zhang, J.; Yue, J.; Tan, Y.; Zhang, D.; Zhang, Q.; Wang, Q. Construction and Application of 3D Borehole Visualization System. *Coal Technol.* **2017**, *36*, 106–108.

26. Fan, K. Application of 3D Visualization of Gas Drainage Borehole in Sihe Coal Mine. *Coal Technol.* **2017**, *36*, 185–187.

27. Zhu, Q.; Zhang, Z.; Liang, J.; Liu, X.; Gu, L.; Zhong, L. Fast generation method of 3D mine roadway model and its application. *China Saf. Sci. J.* **2022**, *32*, 48–57.

28. Zhang, F.; Shang, W.; Luo, H.; Wang, N.; Jia, J.; Li, B. Analysis on influential factors of effective radius of gas extraction from coal seam borehole. *Min. Saf. Environ. Prot.* **2022**, *49*, 137–142.

29. Tang, G.; Sheng, J.; Wang, D.; Men, S. Continuous Estimation of Human Upper Limb Joint Angles by Using PSO–LSTM Model. *IEEE Access* **2021**, *9*, 17986–17997. [CrossRef]

30. Xu, Y.; Hu, C.; Wu, Q.; Jian, S.; Li, Z.; Chen, Y.; Zhang, G.; Zhang, Z.; Wang, S. Research on Particle Swarm Optimization in LSTM Neural Networks for Rainfall–Runoff Simulation. *J. Hydrol.* **2022**, *608*, 127553. [CrossRef]

31. Gao, J.W.; Jia, Z.H.; Wang, X.Y.; Xing, H. Degradation trend prediction of proton exchange membrane fuel cell based on PSO–LSTM. *J. Jilin Univ. (Eng. Technol. Ed.)* **2022**, *52*, 2192–2202.

32. Yang, G.; Zhu, Q.; Wang, D.; Feng, Y.; Chen, X.; Li, Q. Method and Validation of Coal Mine Gas Concentration Prediction by Integrating PSO Algorithm and LSTM Network. *Processes* **2024**, *12*, 898. [CrossRef]